



ELSEVIER

Contents lists available at ScienceDirect

## Computer Aided Geometric Design

www.elsevier.com/locate/cagd

On pseudo-harmonic barycentric coordinates<sup>☆</sup>Renjie Chen<sup>a,\*</sup>, Craig Gotsman<sup>b</sup><sup>a</sup> Max Planck Institute for Informatics, Saarbrücken, Germany<sup>b</sup> Jacobs Technion–Cornell Institute, Cornell Tech, New York, USA

## ARTICLE INFO

## Article history:

Received 4 November 2015

Received in revised form 21 April 2016

Accepted 23 April 2016

Available online xxxx

## Keywords:

Barycentric coordinates

Harmonic functions

Moving least squares

Kernel functions

## ABSTRACT

Harmonic coordinates are widely considered to be perfect barycentric coordinates of a polygonal domain due to their attractive mathematical properties. Alas, they have no closed form in general, so must be numerically approximated by solving a large linear equation on a discretization of the domain. The alternatives are a number of other simpler schemes which have closed forms, many designed as a (computationally) cheap approximation to harmonic coordinates. One test of the quality of the approximation is whether the coordinates coincide with the harmonic coordinates for the special case where the polygon is close to a circle (where the harmonic coordinates have a closed form – the celebrated Poisson kernel). Coordinates which pass this test are called “pseudo-harmonic”. Another test is how small the differences between the coordinates and the harmonic coordinates are for “real-world” polygons using some natural distance measures.

We provide a qualitative and quantitative comparison of a number of popular barycentric coordinate methods. In particular, we study how good an approximation they are to harmonic coordinates. We pay special attention to the Moving-Least-Squares coordinates, provide a closed form for them and their transfinite counterpart (i.e. when the polygon converges to a smooth continuous curve), prove that they are pseudo-harmonic and demonstrate experimentally that they provide a superior approximation to harmonic coordinates.

© 2016 Elsevier B.V. All rights reserved.

## 1. Introduction

## 1.1. Polygon barycentric coordinates

Barycentric coordinates were developed primarily for interpolation purposes, the most common scenario being the interpolation of a real function given on the boundary of a two-dimensional polygon, where the values of the function are specified on the polygon vertices, and assumed to vary linearly between these values along the edges. The objective is then to associate with any interior point in the polygon a real value which is some natural combination of the values given at the vertices.

More precisely, let  $P$  be a planar polygon with vertices  $p_j = (x_j, y_j)$ ,  $j = 1, \dots, n$ . Given real values  $f_j$  at  $p_j$ , what should be the value  $f(x, y)$  associated with a point  $(x, y) \in \text{int}(P)$  (interior to  $P$ )? To answer this, we associate with each vertex

<sup>☆</sup> This paper has been recommended for acceptance by Kai Hormann.

\* Corresponding author.

E-mail address: [renjie.c@gmail.com](mailto:renjie.c@gmail.com) (R. Chen).

$p_j$  a barycentric coordinate function  $B_j(x, y)$  which satisfies a number of natural conditions, and then define

$$f(x, y) = \sum_{j=1}^n f_j B_j(x, y). \quad (1)$$

The conditions that the  $B_j$  are required to satisfy are:

- C1. Non-negativity:  $B_j(x, y) \geq 0$ ,  $j = 1, \dots, n$ ,  $\forall (x, y) \in \text{int}(P)$
- C2. Constant precision:  $\sum_{j=1}^n B_j(x, y) = 1$ ,  $\forall (x, y) \in \text{int}(P)$
- C3. Linear precision:  $\sum_{j=1}^n x_j B_j(x, y) = x$ ,  $\sum_{j=1}^n y_j B_j(x, y) = y$ ,  $\forall (x, y) \in \text{int}(P)$
- C4. Lagrange property:  $B_j(p_k) = \delta_{jk}$

The main advantage of using barycentric coordinates is that the coordinate functions  $B_j(x, y)$  depend only on the polygon  $P$ , and not on the  $f_j$ , so may be pre-computed. Thus a change in any of the  $f_j$  can be reflected easily in  $f(x, y)$  as a simple linear combination.

In the field of computer graphics, barycentric coordinates have been used to generate mappings between two-dimensional regions by associating a 2D vector value  $q_j = (u_j, v_j)$  with each vertex of  $P$  instead of the usual scalar value  $f_j$ . This means that the edges of the *source* polygon  $P = (p_1, \dots, p_n)$  are linearly mapped to the edges of the *target* polygon  $Q = (q_1, \dots, q_n)$  and the barycentric coordinate functions define the image of an interior point  $(x, y) \in \text{int}(P)$ :

$$u(x, y) = \sum_{j=1}^n u_j B_j(x, y)$$

$$v(x, y) = \sum_{j=1}^n v_j B_j(x, y)$$

The barycentric mapping inherits the properties of the coordinate functions used. Over the years, many recipes for  $B_j(x, y)$  have been proposed, the simplest and most well-known being the Laplace (also called *discrete harmonic* or *cotangent*) (Pinkall and Polthier, 1993), mean value (Floater, 2003; Hormann and Floater, 2006) and Wachspress (1975) coordinates. These have simple closed-form expressions for any interior point, so are easy to compute. Alas, they are so simple that they do not behave well on domains with complicated shapes, most notably the Laplace and Wachspress coordinates generate very bad mappings of non-convex domains. Indeed, for many polygons (even convex) they actually violate condition C1 (non-negativity).

Probably the most desirable barycentric coordinate functions are those which generate the unique harmonic mapping between the source and target with the given piecewise linear boundary conditions. Harmonic mappings are desirable since they have many attractive mathematical properties beyond C1–C4, such as smoothness, satisfaction of maximum and minimum principles, the mean-value property and minimization of Dirichlet energy. Another very important property is that harmonic mappings onto convex polygons are guaranteed to be bijective. When used in the Finite-Element Method (FEM), harmonic elements are considered a natural generalization of the linear basis functions on triangles and the bilinear basis functions on quads, and retain almost all their desirable properties even for non-convex elements (Martin et al., 2008). For all these reasons, harmonic maps of polygonal domains have been used in many 2D and 3D deformation applications (Ben-Chen et al., 2009; Schneider and Hormann, 2015). Unfortunately, the harmonic barycentric coordinate functions (first used in Joshi et al., 2007) have no closed form for general polygons and must be computed numerically by solving a discrete Laplace equation with appropriate Dirichlet boundary conditions on  $P$ . This requires a finite-element (FEM) discretization of the interior of  $P$ , typically by dense triangulation. Although sparse, the resulting linear system, whose size is proportional to the number of finite elements, can be very large, so slow to solve. The result is a piecewise-linear approximation to the coordinate functions on  $P$ , albeit with perfect satisfaction of the boundary conditions. Alternative numerical methods (e.g. Weber and Gotsman, 2010) use boundary elements (BEM), which results in perfect harmonic functions on the domain at the price of approximate satisfaction of the boundary conditions. These methods also involve the solution of a dense (though not too large) system of linear equations. Beyond the significant computation complexity, another disadvantage of the harmonic coordinates relative to the simple others mentioned above is that it is impossible to compute the coordinates of just a *single* point in the domain without computing the coordinates of *all* (sampled) domain points.

Since the harmonic barycentric coordinates are so important, a number of methods whose primary objective is to approximate the harmonic coordinates, were invented. These include the mean-value coordinates and others, details of which we will provide later. Of special interest are the so-called Moving Least-Squares (MLS) coordinates (Manson and Schaefer, 2010), which have a closed form requiring not much more computation than, say, mean-value coordinates, but as we will show, generate a superior approximation to harmonic coordinates. The interested reader is also referred to the recent survey by Floater (2015) for a comprehensive overview of many barycentric coordinate recipes.

A simple test for the quality of approximation of a given barycentric coordinate scheme to the harmonic coordinates is the behavior of the coordinates in the special case where the polygon has a very large number of vertices and converges

in shape to a circle. In the case of a circle, the harmonic coordinates have a well-known closed form, the so-called *Poisson kernel* (Ahlfors, 1979), and if the barycentric coordinates in question converge to this form, we say that the coordinates are “pseudo-harmonic”. However, in order to be more precise when talking about barycentric schemes on smooth continuous domains such as the disk (instead of discrete polygons), we need to recall the concept of *transfinite* barycentric coordinates, which we do in the next section. After that we will be in a position to state our results more precisely.

### 1.2. Transfinite barycentric coordinates

The concept of barycentric coordinates of a polygon  $P$  with a finite set of vertices may be generalized to a closed simple planar curve  $S$ , which may be thought of as the limit of a polygon with an increasing number of vertices. In this case the discrete index  $j$  (over the vertices) in the sum (1) becomes a continuum, the value of  $f$  is given at a continuum of points of  $S$ , the discrete sum is replaced by a contour integral, and the finite set of barycentric coordinate functions is replaced by a real-valued *kernel* function  $K(s, t)$ , where  $s$  is a 2D point on  $S$ ,  $t$  is a 2D point in the interior of  $S$ . Eq. (1) then becomes:

$$f(t) = \oint_S K(s, t) f(s) ds \tag{2}$$

meaning that the value of  $f$  at an interior point  $t$  is defined to be some weighted average of the values of  $f$  given on the boundary  $S$ . The kernel  $K$  should typically be smooth and satisfy conditions analogous to conditions C1–C3 above:

- D1. Non-negativity:  $K(s, t) \geq 0, \forall s \in S, \forall t \in \text{int}(S)$
- D2. Constant precision:  $\oint_S K(s, t) ds = 1, \forall t \in \text{int}(S)$
- D3. Linear precision:  $\oint_S sK(s, t) ds = t, \forall t \in \text{int}(S)$

Perhaps the most well-known transfinite barycentric kernel is the so-called *Poisson kernel* (Ahlfors, 1979) mentioned above. This kernel  $K_P$  reproduces harmonic functions, but only when the domain is the *unit disk*:

$$K_P(s, t) ds = \frac{ds}{\|s - t\|^2} \tag{3}$$

The  $ds$  differential is the standard (and default) arc-length differential, as opposed to other differentials (such as  $d\theta$  and  $dw$  that we will employ later). We write it explicitly when needed to avoid confusion. Transfinite barycentric kernels have been investigated by Belyaev (2006) and others (e.g. Schaefer et al., 2007; Dyken and Floater, 2009; Kosinka and Barton, 2016). They were able to describe the kernels which are the transfinite counterparts of some of the well-known discrete (polygon) barycentric coordinate recipes. For example, Belyaev (2006) shows that one of the most basic recipes are the mean value coordinates, and the others are generalizations of this basic form. However, Belyaev’s formulation (Belyaev, 2006) is complicated somewhat by the fact that the integral (2) is taken not over the contour  $S$ , rather over a “virtual” unit circle centered at  $t$ :

$$f(t) = \oint_S K(s, t) f(s) d\theta$$

where  $\theta$  is the angle formed by the ray through  $s$  originating at  $t$ , in effect traversing the unit circle around  $t$ . With this differential, it turns out that the mean-value kernel is just the (normalized) inverse distance:

$$K_{MV}(s, t) d\theta = \frac{d\theta}{\|s - t\|} \tag{4}$$

A practical question is how to convert transfinite barycentric kernels to their finite barycentric coordinate functions counterparts in the case that the contour  $C$  is actually a polygon. This is relatively simple. Given a transfinite barycentric kernel  $K(s, t)$ , if the contour is an  $n$ -sided polygon  $P$  with vertices  $(p_1, \dots, p_n)$ , then the kernel may be converted into  $n$  barycentric coordinate functions  $B_j$ , one for each vertex, in the following manner:

$$B_j(t) = \int_{r=0}^1 rK(p_{j-1} + r(p_j - p_{j-1}), t) \|p_j - p_{j-1}\| dr + \int_{r=0}^1 rK(p_{j+1} + r(p_j - p_{j+1}), t) \|p_j - p_{j+1}\| dr \tag{5}$$

reflecting the fact that the polygon is given with data values on its vertices, which are assumed to vary linearly over the edges (meaning that the image of  $P$  is also a polygon).

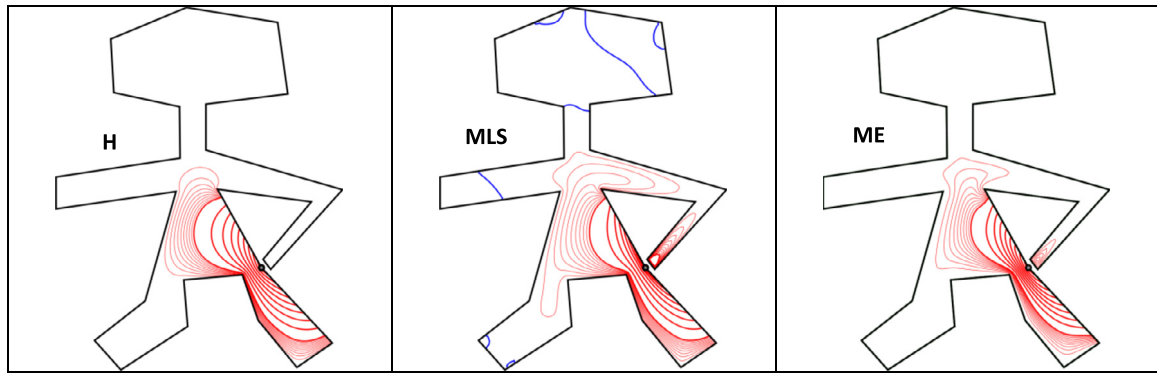


**Fig. 1.** Barycentric coordinate functions of the marked vertex of a non-convex polygon. Left to right: Harmonic (H), Moving Least Squares (MLS), Maximum Entropy (ME). According to our numerical experiments, MLS and ME are the closest approximations to H. Other coordinate functions are provided in Fig. 7.

## 2. Our objective

In this paper we investigate the quality of approximation afforded by a number of popular barycentric coordinate schemes to the harmonic coordinates. In particular, we systematically analyze two variants of the Moving Least Squares (MLS) coordinates, introduced by [Manson and Schaefer \(2010\)](#). We provide the kernel function for their transfinite versions and prove that they are pseudo-harmonic. We also demonstrate experimentally that, based on a number of metrics that we propose, they are the best approximation to harmonic coordinates on many types of polygons, compared to other known coordinate schemes. For example, Fig. 1 shows the contour lines of the harmonic, Moving Least Squares and Maximum Entropy barycentric coordinate functions associated with a vertex of a typical non-convex polygon. The latter two are shown to be excellent numerical approximations to the harmonic function.

## 3. Pseudo-harmonic transfinite barycentric kernels

Many of the barycentric coordinate recipes were invented in an attempt to approximate the harmonic coordinates, which in general have no closed form and must be computed numerically. The quality of the approximation is typically better if more computation is invested, resulting in somewhat more complicated formulae. One basic test of the quality of the approximation is when the contour is the simplest possible – the unit circle  $C$ . In this case it is well known that the harmonic kernel is the so-called *Poisson kernel* ([Ahlfors, 1979](#)), given in complex number algebra as:

$$K_P(w, z)ds = \frac{1}{2\pi} \operatorname{Re} \left( \frac{w+z}{w-z} \right) ds = \frac{1}{2\pi} \frac{1-|z|^2}{|w-z|^2} ds \quad (6)$$

where  $w$  is a point on the circle  $C$  and  $z$  an interior point within the circle. It is possible to superficially simplify this formula by noticing that some of it is a function of  $z$  only, thus may be omitted, resulting in the complex analog to (3):

$$K_P(w, z)ds = \frac{ds}{|w-z|^2} \quad (7)$$

and recovered as part of a standard normalization procedure, i.e. given boundary values  $f(w)$ , the Dirichlet problem on the unit disk may be solved as

$$f(z) = \frac{\oint_C K_P(w, z) f(w) ds}{\oint_C K_P(w, z) ds}$$

Note that  $ds$  is still the arc-length boundary element  $ds = |dw|$ , where  $dw$  is the more common differential used in complex analysis.

If a given transfinite barycentric coordinate scheme reduces to the Poisson kernel for the special case that the contour is the unit circle, we say that the coordinates are *pseudo-harmonic*. [Belyaev \(2006\)](#) has shown that the popular special cases of three-point coordinates (described in Section 4.1 below), in the continuous limit, are not pseudo-harmonic, but those introduced by [Gordon and Wixom \(1974\)](#) (see Section 4.4 below) are.

## 4. Some barycentric coordinate schemes

In this section we provide some necessary details on a number of popular barycentric coordinate schemes that we will later compare. We will prefer to use the complex number formulation.

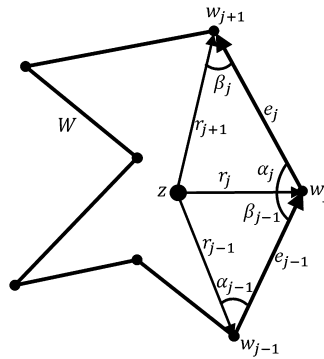


Fig. 2. The terminology of complex barycentric coordinates.

4.1. The “three-point” coordinates

In the 2D scenario, it is convenient to represent 2D vectors  $(x, y) \in \mathbb{R}^2$  as complex numbers  $z \in \mathbb{C}$ . Using this formulation, Weber et al. (2009) showed that it is possible to express any barycentric coordinate function as complex-valued functions:

$$\hat{B}_j(z) = \gamma_j(z) \frac{r_{j+1}(z)}{e_j} - \gamma_{j-1}(z) \frac{r_{j-1}(z)}{e_{j-1}}, \quad B_j(z) = \frac{\hat{B}_j(z)}{\sum_{j=1}^n \hat{B}_j(z)} \tag{8}$$

where  $W = (w_1, \dots, w_n)$  are the source polygon vertices,  $z$  is a point in the interior of the source polygon,  $r_j(z)$  is the difference  $w_j - z$ ,  $e_j$  is the edge vector  $w_{j+1} - w_j$  and  $\gamma_j$  is a complex-valued function associated with the  $j$ 'th edge. See Fig. 2. Thus the mapping of the interior of the source polygon to the interior of the target polygon whose vertices are  $f_j$ ,  $j = 1, \dots, n$  is

$$f(z) = \sum_{j=1}^n B_j(z) f_j$$

Weber et al. (2011) show that the popular special cases of the so-called “three-point coordinates” – Wachspress (W), mean-value (MV) and Laplace (L) – may be obtained for

$$\gamma_j(z) = \frac{e_j}{\text{Im}(\bar{r}_j(z)r_{j+1}(z))} \left( \frac{|r_{j+1}(z)|^p}{r_{j+1}(z)} - \frac{|r_j(z)|^p}{r_j(z)} \right) \tag{9}$$

with  $p = 0, 1, 2$ , respectively. We remind the reader that  $\bar{z}$  is the complex conjugate of  $z$ .

The advantage of using the complex formulation is that many of the formulae become very simple. For example, Weber et al. (2009) showed that the so-called Green coordinates introduced by Lipman et al. (2008) to generate conformal mappings may be expressed very simply in the complex formulation, essentially using the very simple kernel  $K_C(w, z)dw = \frac{dw}{w-z}$  featuring in Cauchy’s integral formula (Ahlfors, 1979) (with the complex differential  $dw$ ).

Given a simple planar polygon  $W$  having vertices (in complex form)  $w_j$ ,  $j = 1, \dots, n$ , the three-point schemes express  $B_j(z)$  – the un-normalized barycentric coordinate function associated with  $w_j$  as a function of just  $w_{j-1}$ ,  $w_j$ ,  $w_{j+1}$  (and of course  $z$ ). This is reflected also in (8). For example, the Laplace coordinate function is just the sum of the cotangents of the two angles formed by  $(w_j, w_{j-1}, z)$  and  $(w_j, w_{j+1}, z)$ :  $\alpha_{j-1}$  and  $\beta_j$  in Fig. 2. Similarly, the mean-value and Wachspress coordinates involve only angles and edge lengths in these two triangles.

The mean-value (MV) coordinates are particularly interesting as they are derived by trying to mimic the mean-value property of harmonic functions (Floater, 2003; Hormann and Floater, 2006). Yet, as Belyaev (2006) notes, they are not pseudo-harmonic, and neither are the Wachspress (W) or Laplace (L) coordinates. In contrast, when the polygon is a unit square, both the Wachspress and Laplace coordinates are exactly the harmonic bilinear coordinates:

$$B_1(x, y) = (1 - x)(1 - y), \quad B_2(x, y) = x(1 - y), \quad B_3(x, y) = (1 - x)y, \quad B_4(x, y) = (1 - x)(1 - y)$$

This was noted by Floater et al. (2006), who also noted that these two coordinates coincide for any circular polygon (sometimes called a cyclic polygon), i.e. a polygon whose vertices all lie on a circle, including the regular polygons (those having equal edge lengths). Floater et al. (2006) also observed that the Laplace coordinates are positive for all interior points of a polygon iff the polygon is circular. Thus the Laplace coordinates will incur negative values on almost all polygons, even those which are convex, quite unlike most of the other coordinate schemes, who are typically non-negative on convex polygons. More properties of the transfinite mean-value coordinates were provided by Dyken and Floater (2009) and the rates of convergence of finite mean value coordinates (and others) on a polygon to their transfinite counterparts was studied by Kosinka and Barton (2016).

#### 4.2. Harmonic ( $H$ ) coordinates

When interpolating boundary values given on a contour, the typical objective is that the interpolated value at an interior point  $z$  is some convex combination of the boundary values  $f(w)$ , where the weight of boundary point  $w$  is (obviously) positive, and inversely proportional to some “distance” between  $z$  and  $w$ . Ideally this reflects the distance *within* the contour, as opposed to the simple Euclidean distance which ignores the contour, and the two may be quite different if the contour is non-convex and convoluted. A harmonic interpolant, which is known to exist for any given boundary values (the solution to the so-called Dirichlet problem), provides this effect of “interior” distance, and may be obtained by solving the Laplace second-order differential equation on the domain. In general, except for a few special contours, there is no closed-form solution to this equation, and its solution must be computed numerically. This involves discretizing the interior of the contour (usually by a Finite-Element triangulation) and solving the discrete linear Laplace equation with the appropriate boundary values. If the contour is a polygon with  $n$  vertices, each of the  $n$  barycentric coordinate functions may be computed separately, where the boundary values for the  $j$ 'th coordinate function is linear increasing between 0 and 1 on the edge  $[w_{j-1}, w_j]$  and linearly decreasing between 1 and 0 on the edge  $[w_j, w_{j+1}]$ . Everywhere else it is 0. This means that the value of the coordinate function for a single interior point cannot be computed independently of all the other interior points (sampled in the discretization). Thus, even though the resulting linear systems are sparse, their solution typically involves significant computation. Alternatively, Boundary-Element Methods (BEM) (e.g. [Weber and Gotsman, 2010](#)), whose complexity is proportional to the size of the discretization of the boundary, which is typically much less than the size of the discretization of the interior, may be used to produce an accurate harmonic function on the interior, at the expense of fully interpolating the given boundary values. **In the transfinite case, the harmonic kernel is known in closed form only for very few simple boundaries, including the unit circle, where it is known as the Poisson kernel** (see Section 3).

#### 4.3. Poisson ( $P$ ) coordinates

Poisson coordinates ([Li and Hu, 2013](#)) (not to be confused with the Poisson kernel) are derived in a manner similar to mean-value coordinates, except that instead of using the mean-value property of harmonic functions, which is applicable only to a point at the *center* of a circle, the Poisson kernel is used to approximate the value of the function at an arbitrary point within a circle. Together with an elaborate method for positioning the circle for a given interior point  $z$ , this results in a pseudo-harmonic coordinate system.

#### 4.4. Gordon–Wixom ( $GW$ ) coordinates

One of the earliest transfinite barycentric schemes is due to [Gordon and Wixom \(1974\)](#). This expresses the kernel value between interior point  $z$  and contour point  $w$  in terms of  $z$ ,  $w$  and  $w_1$ , where  $w_1$  is the antipode of  $w$  with respect to  $z$ , i.e. the point on the contour intersected by the ray originating at  $z$ , proceeding in the direction *opposite* that of  $w$ . For a convex contour – the case dealt by Gordon and Wixom –  $w_1$  is unique. Gordon and Wixom proved that this scheme is pseudo-harmonic. These coordinates were later generalized by [Belyaev \(2006\)](#) to the non-convex case (essentially taking into account *all* the points of intersection of a line through  $z$  with the contour), retaining the pseudo-harmonicity, but losing the positivity of the coordinates.

#### 4.5. Positive Gordon–Wixom ( $PGW$ ) coordinates

[Belyaev \(2006\)](#) also defined weighted versions of the Gordon–Wixom coordinates, which, under mild conditions on the weighting function, are still pseudo-harmonic. In a followup work, [Belyaev and Fayolle \(2015\)](#) showed that certain weighting functions could lead to better approximation of the harmonic coordinates. Similarly, [Mason and Schaefer \(2011\)](#) described the so-called *positive Gordon–Wixom* ( $PGW$ ) coordinates based on very specific weighting functions. These are non-negative everywhere, even on non-convex contours, but unfortunately no longer pseudo-harmonic.

#### 4.6. Maximum Entropy ( $ME$ ) coordinates

In the quest for non-negative barycentric coordinates for all types of contours, [Sukumar \(2004\)](#) and [Hormann and Sukumar \(2008\)](#) formulated the coordinates for a given interior point  $z$  as the solution to an optimization problem, which involves maximizing an entropy function involving all the boundary values. This is borrowed from probability theory, where probabilities are always non-negative. Being a convex function, the entropy is amenable to robust numerical optimization and has a unique global minimum. Different coordinates may be generated when using different *prior* functions. [Sukumar \(2004\)](#) showed that for a constant prior,  $ME$  coordinates reproduce the harmonic (bilinear) coordinates on the unit square. Unfortunately, this is not the case for the unit circle. [Hormann and Sukumar \(2008\)](#) later introduced a number of other geometric priors, one which would seem to also reproduce the harmonic function on the square.

#### 4.7. Moving Least-Squares (MLS) coordinates

In a very interesting paper, [Manson and Schaefer \(2010\)](#) defined the Moving Least-Squares (MLS) barycentric coordinates for polygons, to be used primarily in a 2D mapping scenario. The starting point is an *influence function*  $R(w, z)$  (not to be confused with a kernel function) which, for every  $w$  on the source contour  $S$ , defines its influence on a point  $z$  interior to  $S$ . Typical influence functions are  $|w - z|^{-2\alpha}$ , with integer  $\alpha \geq 1$ . Assume we are also given a target contour  $T$  corresponding to  $S$ . Then, given a point  $z$  interior to  $S$ , an affine transformation  $A_z$ , which best maps the points  $w \in S$  to their corresponding points  $f(w) \in T$ , is computed using weighted least-squares, where each point  $w \in S$  is weighted by  $R(w, z)$ . The image of  $z$ , namely  $f(z)$ , is then defined to be  $A_z(z)$ . Computation of  $A_z$  is linear in the number of points on the source contour  $S$ , and this results in the complete set of barycentric coordinate values for  $z$ . Note that even the simple three-point coordinates (L, MV, W) require linear time to compute the analogous set of values for a given  $z$  (because they must be normalized).

It turns out that  $f(z)$ , as defined by the MLS procedure, may be expressed using a transfinite barycentric kernel. As we show in [Theorem A.1](#) in [Appendix A](#), for the natural influence function  $R(w, z) = |w - z|^{-2}$  (i.e.  $\alpha = 1$ ), when the requirement of an *affine* transformation is replaced by the requirement of a *similarity* transformation, we obtain the very simple (un-normalized) transfinite barycentric kernel  $K_{SMLS}(w, z)$  (for the  $ds$  differential):

$$K_{SMLS}(w, z) = \frac{P}{|w - z|^2} - \frac{Q(z)}{w - z} \quad (10)$$

where  $P$  is the length of  $S$  and

$$Q(z) = \oint_S \frac{1}{w - z} ds$$

is a function of  $z$  only that involves an integral over the entire contour. This kernel is complex-valued and is guaranteed to reproduce only similarity transformations of  $S$  to  $T$  (as opposed to general affine transformations). [Theorem A.4](#) in [Appendix A](#) gives a closed-form expression for  $Q(z)$  in the case that the contour is a polygon, by computing the integrals of (5).

The affine case is a little more difficult to analyze. It is convenient to transform the plane by a similarity transformation, which simplifies the computations. In [Theorem A.2](#) of [Appendix A](#), we show that the affine-based MLS kernel for the natural influence function  $R(w, z) = |w - z|^{-2}$ , after a simplifying similarity transformation of the plane, is

$$K_{AMLS}(w, z) = \frac{1}{|w - z|^2} + 2 \frac{A(z) \operatorname{Re}(w\bar{z}) - B(z) \operatorname{Re}(wz)}{A^2(z) - B^2(z)} \frac{1}{|w - z|^2} \quad (11)$$

where

$$A(z) = \oint_S \frac{w}{w - z} ds \quad \text{and} \quad B(z) = \oint_S \frac{\bar{w}}{w - z} ds$$

### 5. Pseudo-harmonicity of the MLS coordinates

[Manson and Schaefer \(2010\)](#) did not provide the transfinite version of the MLS coordinates, thus did not investigate whether the MLS coordinate scheme is pseudo-harmonic. In fact, other authors ([Li and Hu, 2013](#)) seem to believe it is not. This is probably because they mainly concentrate on the case  $\alpha = 2$ . However, we show in [Theorem A.3](#) in [Appendix A](#) that both the affine-based and the similarity-based MLS kernels for the more natural case  $\alpha = 1$  are indeed pseudo-harmonic. The essence of the proofs is to prove that the second terms in (10) and (11) vanish when  $S$  is a circle. Furthermore, our experimental results (see [Section 6](#)) show that the affine-based MLS kernel is an excellent approximation to the harmonic kernel for a variety of polygons.

### 6. Experimental comparison

We have generated the barycentric coordinates described in [Section 4](#) for a number of interesting polygons and compared the quality of their approximation to the harmonic coordinates. The polygons were the unit square, the unit circle (approximated as a regular polygon with 48 edges), an irregular convex pentagon, a highly non-convex polygon with 25 edges shaped like a human figure, and a variant on the same polygon with 27 edges, where one part of the polygon (the hand) bends back to come very close to another unrelated part of the polygon (the hip). [Figs. 3–7](#) show some of the resulting basis functions. Specifically, we show a contour plot of a select basis function. The thick red contour lines are spaced at 0.1, and the thin ones at 0.01. The thick blue contour is the zero crossing.

We are especially interested in how good an approximation the various coordinate functions are to the holy grail – the harmonic coordinate function. We measure this using three different error functions:

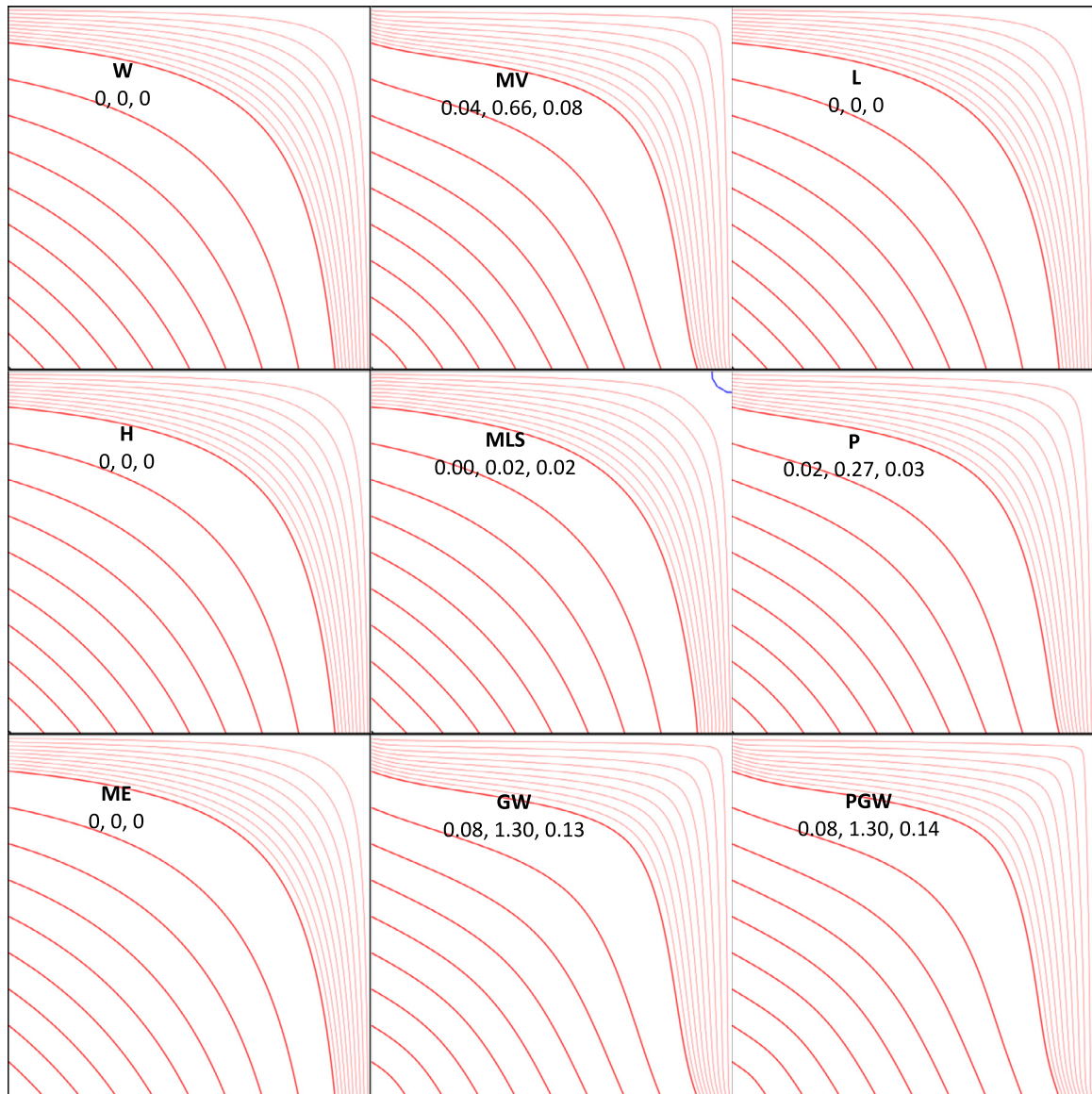


**Fig. 3.** Barycentric coordinate function of the bottom-left vertex of a square. The numbers indicate the errors  $E_1$ ,  $E_2$ ,  $E_3$  of the coordinates relative to the harmonic (H) coordinate function, which is known to be bilinear. Note that the Laplace (L), Wachspress (W) and maximum-entropy (ME) coordinates coincide with the harmonic (H) coordinate, and the (affine) MLS coordinate is extremely close to this, despite the small negative region in the opposite corner.

1. The first error function is the most direct – the relative (squared)  $l_2$  distance between the coordinate function  $B$  and the corresponding harmonic coordinate function  $H$ :

$$E_1(B, H) = \frac{\|B - H\|_2^2}{\|H\|_2^2} = \frac{\iint_{\text{int}(S)} (B(x, y) - H(x, y))^2 dx dy}{\iint_{\text{int}(S)} H(x, y)^2 dx dy}$$

2. Recalling that the harmonic function minimizes the scalar Dirichlet energy (Pinkall and Polthier, 1993) among all functions having given boundary conditions, the second error function measures the relative absolute difference between the Dirichlet energies of the two functions:

$$E_2(B, H) = \frac{|D(B) - D(H)|}{D(H)}$$

3. Recalling that a harmonic function has vanishing Laplacian on the interior, the third error function measures the (squared)  $l_2$  norm of the scalar Laplacian on the interior:

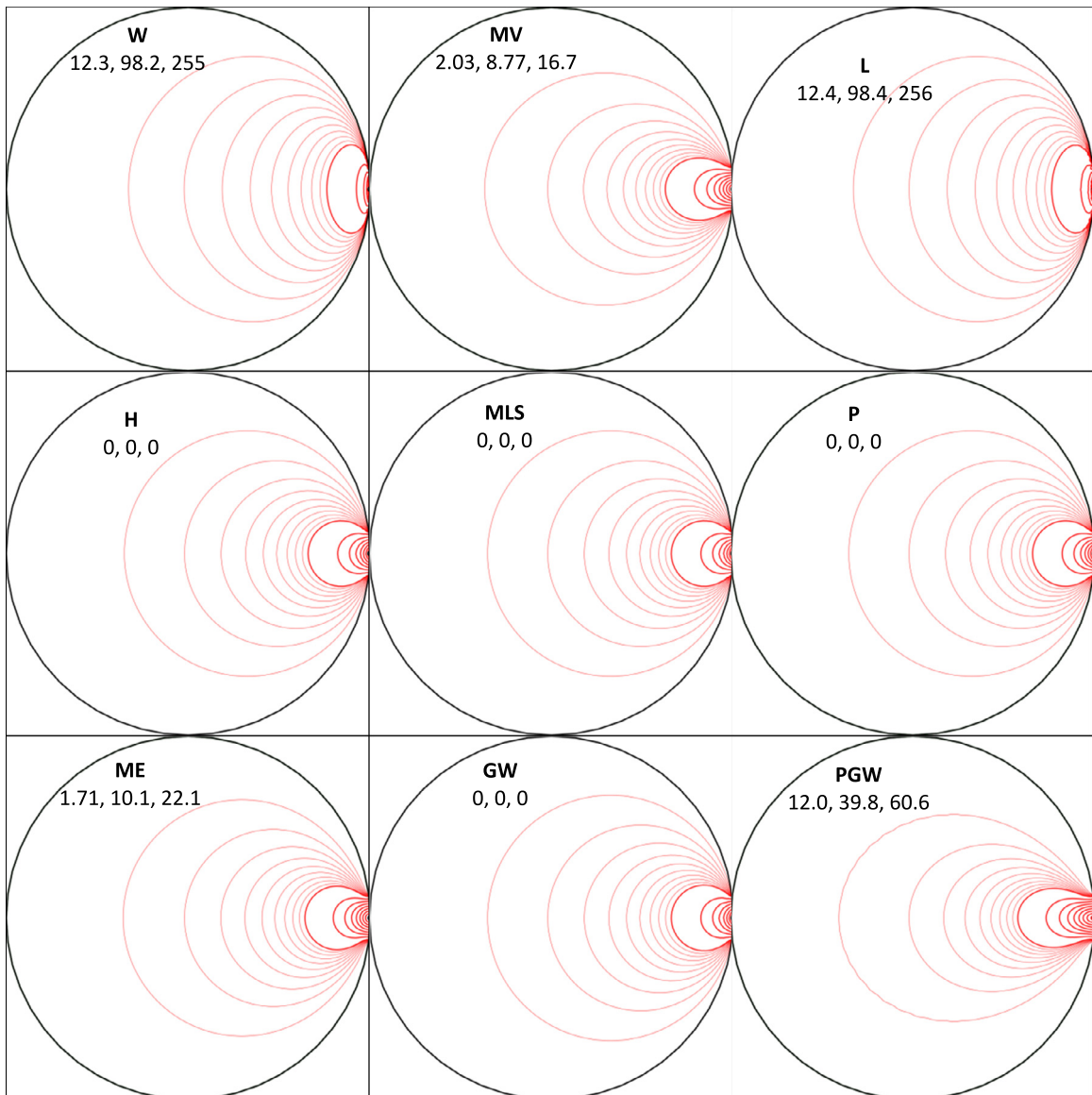


**Fig. 4.** Barycentric coordinate function of a vertex of a regular 48-gon approximating a circle. The numbers indicate the errors  $E_1, E_2, E_3$  of the coordinates relative to the harmonic (H) coordinate function. Note that the (affine) MLS, Gordon–Wixom (GW) and Poisson (P) coordinates are pseudo-harmonic, and the mean-value (MV) and maximum-entropy (ME) coordinates give very good approximations.

$$E_3(B, H) = \|\Delta B\|_2^2 = \iint_{\text{int}(S)} \Delta B(x, y)^2 dx dy$$

In all our examples, the harmonic coordinate function  $H$  was computed numerically by triangulation of the polygon and solution of a linear system of equations over the triangulation vertices. The statistics of the triangulations used are given in Table 1. Thus, in practice, the values of  $H$  are available only at the triangulation vertices and  $H$  is a piecewise-linear function. For compatibility,  $B$  was also computed at the same vertices and an analogous piecewise-linear function formed. Each of the two integrals of  $E_1$  may then be computed as the sum of integrals over triangles, where the function values  $f_1, f_2$  and  $f_3$  given at the vertices of a triangle define a linear interpolant, and the relevant  $l_2$  norm squared is the following integral multiplied by the area of the triangle:

$$\int_0^1 \int_0^{1-\sqrt{r}} ((1-\sqrt{r})f_1 + \sqrt{r}(1-s)f_2 + \sqrt{r}s f_3)^2 dr ds = \frac{1}{6}(f_1^2 + f_2^2 + f_3^2 + f_1 f_2 + f_2 f_3 + f_3 f_1)$$

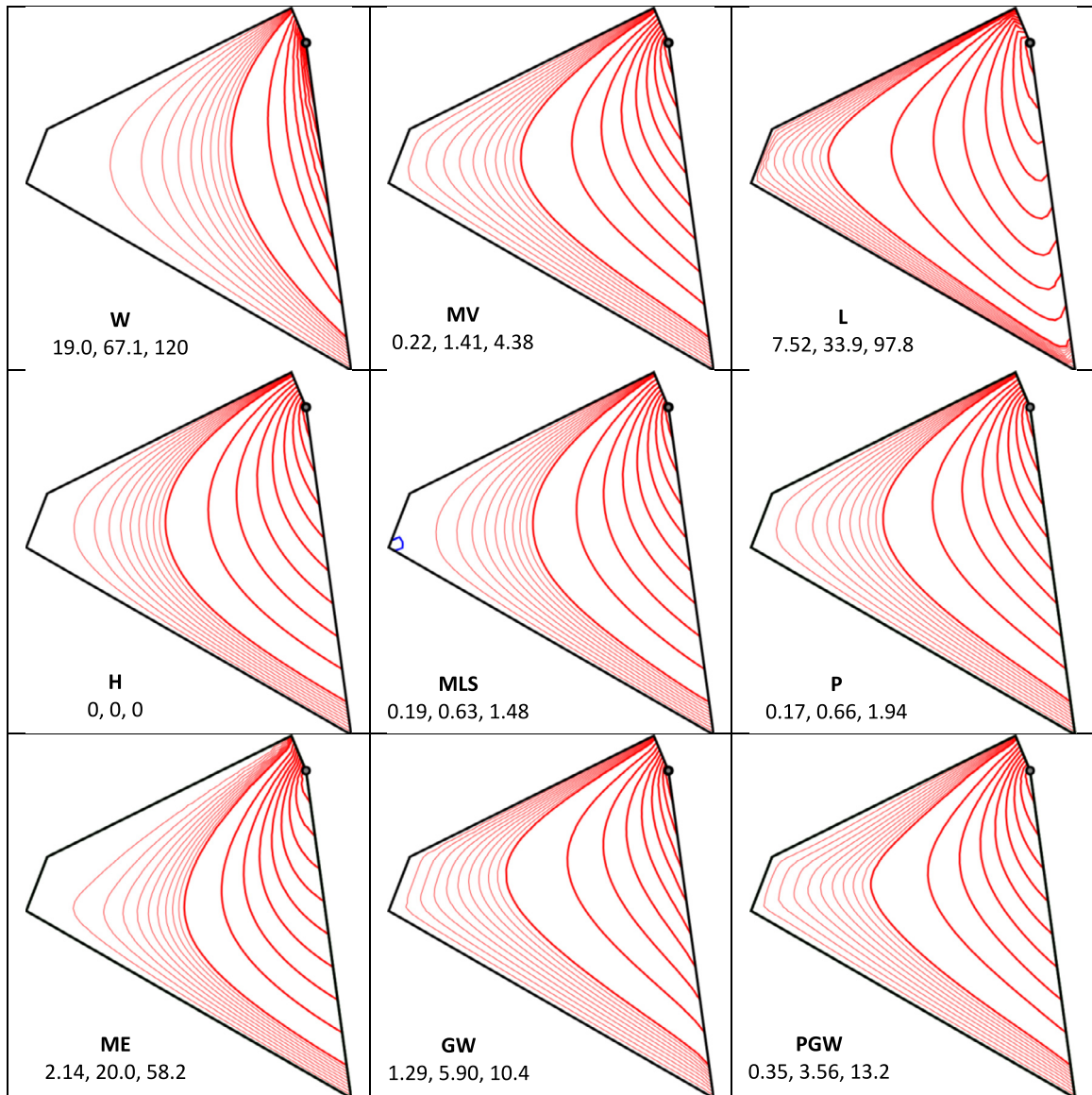


**Fig. 5.** Barycentric coordinate function of the marked vertex of a convex pentagon. The numbers indicate the errors  $E_1$ ,  $E_2$ ,  $E_3$  of the coordinates relative to the harmonic (H) coordinate function. Note the excellent approximation of the harmonic coordinate by the affine MLS coordinate, with the Poisson coordinate a close second.

(the use of  $\sqrt{r}$  and  $s$  induce a uniform density on the triangle). A similar procedure is followed for computation of  $E_3$ , where  $\Delta B$  is numerically evaluated at the interior vertices of the triangulation using the standard cotangent-based Laplacian operator (matrix) (Martin et al., 2008). The Dirichlet energy used in  $E_2$  is also computed as a quadratic form using the same Laplacian matrix.

The tables in Appendix B present the complete set of results: Each of the three error values for each barycentric coordinate function of each test polygon, along with the average for each polygon over all coordinate functions. Since all the coordinate functions of the square and the circle are equivalent (up to rotation), we show the errors on just one such coordinate function. For convenience,  $E_1$  and  $E_2$  are multiplied by  $10^2$  and  $E_3$  is multiplied by  $10^6$ . The \* indicates a resulting value greater than 1,000, which is obviously too large to be of interest.

The experimental results on the first two polygons (Figs. 3–4) confirm some of the theoretical results quoted earlier. The Laplace (L), Wachspress (W) and maximum-entropy (ME) coordinates coincide with the (bilinear) harmonic (H) coordinates on the unit square. None of these are pseudo-harmonic, i.e. coincide with the harmonic coordinates on the unit circle, but the (affine-)MLS, Gordon–Wixom (GW) and Poisson (P) coordinates are. Note that although the MLS coordinates are not identical to the harmonic coordinates on the unit square, they are extremely close, despite the slight negative value in the opposite corner.

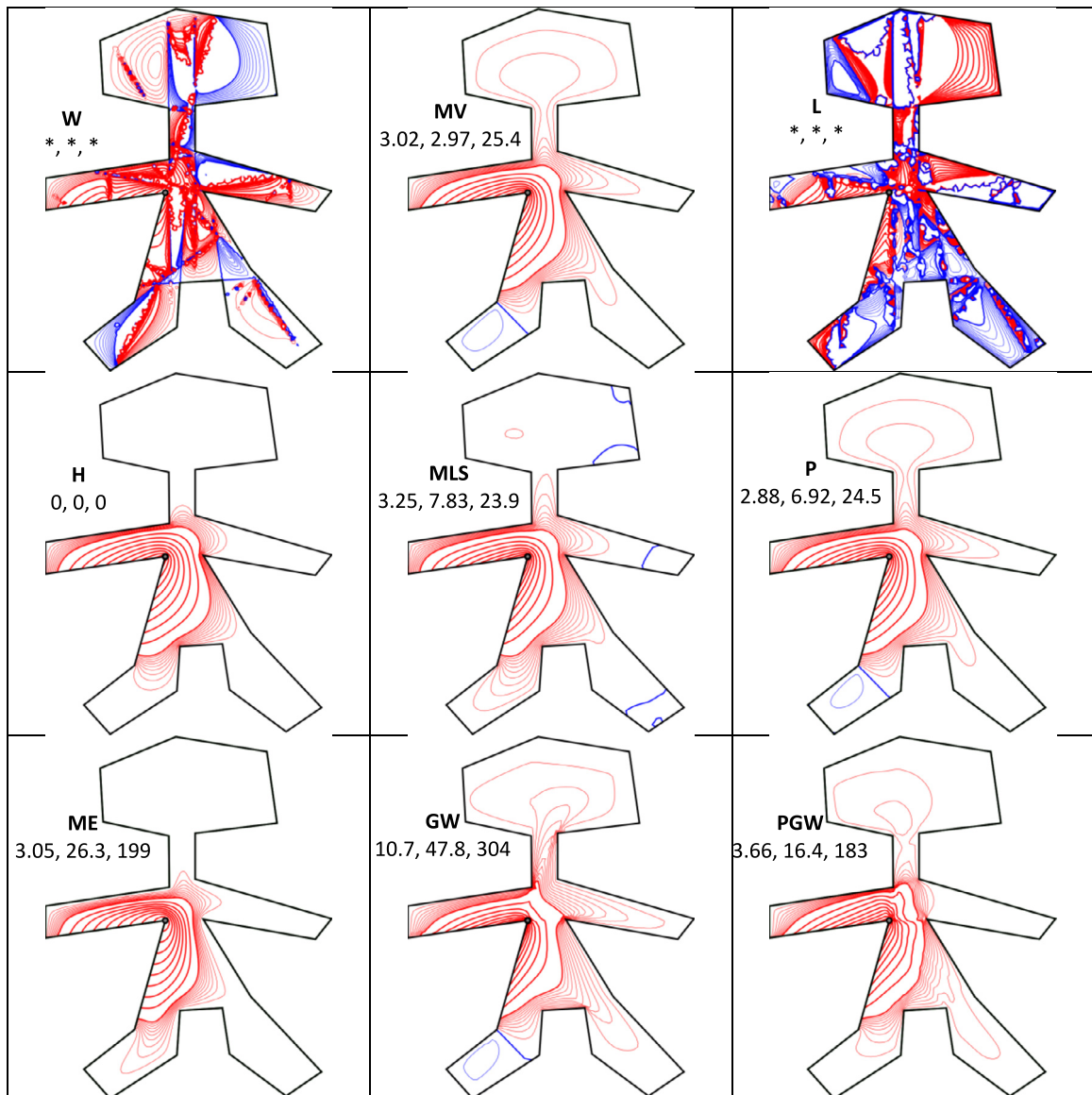


**Fig. 6.** Barycentric coordinate function of the marked vertex of a “man-shaped” non-convex polygon. The numbers indicate the errors  $E_1$ ,  $E_2$ ,  $E_3$  of the coordinates relative to the harmonic (H) coordinate function. Note how bad the Laplace (L) and Wachspress (W) coordinates are and how surprisingly good the mean-value (MV) approximation is.

The results for the irregular convex polygon (Fig. 5) demonstrates that the MLS coordinates are again an excellent approximation to the harmonic coordinates. The Poisson (P) coordinates are a close second.

Figs. 6–7 confirm, as expected, that the Laplace (L) and Wachspress (W) coordinates behave very badly on the non-convex polygons, but the mean-value (MV) coordinates behave surprisingly well.

The most interesting results are in Fig. 7. The right hand of the man figure is very close to the hip, when measured using Euclidean distance. However, when measured using distance through the interior of the polygon, the two pieces of the polygon are actually quite distant. This we would expect the barycentric coordinate function centered at a vertex at the hip to have extremely small values in the hand region. This is evident in the harmonic coordinate function, but not in any of the others, where the coordinate function appears to “leak” from the hip into the hand. This effect seems to be minimal for the maximum-entropy (ME) coordinates.

A more complete picture is given by looking at the average errors per polygon in the tables in Appendix B. These are summarized in Table 1, where for each polygon and error measure averaged over all vertices of the polygon, we have indicated the method which yields the best approximation to the harmonic coordinates. For the square, the W, L and ME coordinates coincide with the harmonic bilinear coordinate functions, thus give zero error. Among all those giving non-zero error, MLS is the smallest for all error measures. For the circle, the MLS, P and GW coordinates are pseudo-harmonic, thus

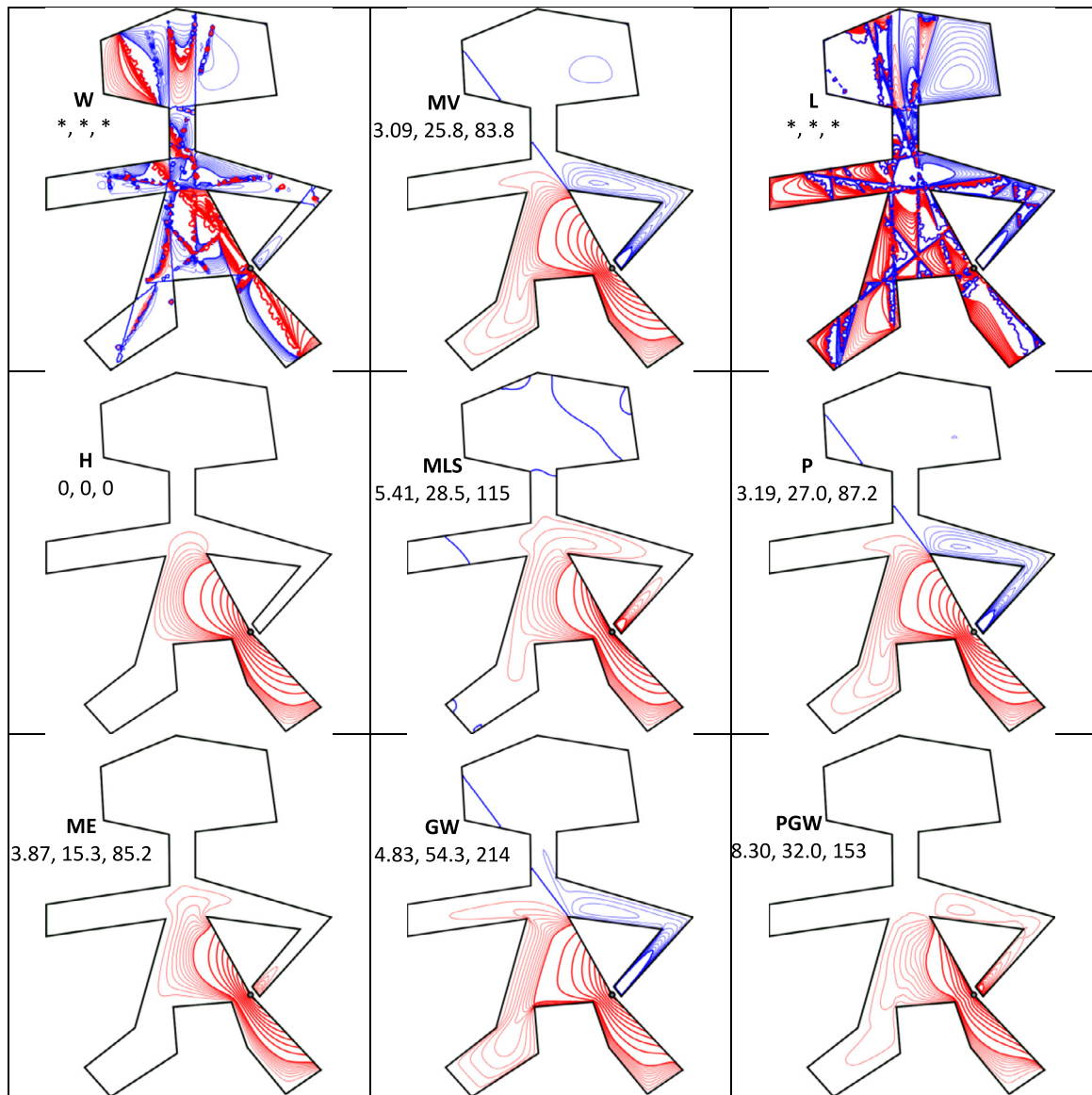


**Fig. 7.** Barycentric coordinate function of the marked vertex of a “man-shaped” non-convex polygon where one hand is very close to the hip. The numbers indicate the errors  $E_1$ ,  $E_2$ ,  $E_3$  of the coordinates relative to the harmonic (H) coordinate function. Note the “leakage” of all the coordinate functions (except the harmonic (H)) from the hip into the hand.

**Table 1**

Discretization statistics and methods best approximating the harmonic (H) barycentric coordinate functions, as derived from the averages in Tables B.1–B.3 in Appendix B.

	Square	Circle	Convex Pentagon	Non-convex Man 1	Non-convex Man 2
Boundary vertices	337	283	144	363	402
Interior vertices	7,584	5,943	1,079	1,441	1,393
Triangles	15,503	12,167	2,300	3,243	3,186
$E_1$	W/L/ME	MLS/P/GW	MLS	MLS	ME
$E_2$	W/L/ME	MLS/P/GW	MLS	MLS	MLS
$E_3$	W/L/ME	MLS/P/GW	MLS	MLS	MLS

coincide with the Poisson kernel, giving zero error. For the non-trivial polygons, especially the non-convex ones, there is overwhelming evidence that the affine-based MLS coordinates are probably the best choice to use as an approximation to the harmonic (H) coordinates.

## Acknowledgements

The first author has been supported by the Max Planck Center for Visual Computing and Communication. We thank Josiah Manson for the use of his software for comparing various barycentric coordinate schemes developed for [Manson and Schaefer \(2010\)](#) and Xian-Ying Li for the use of his software implementing Poisson coordinates ([Li and Hu, 2013](#)).

## Appendix A

In this Appendix we develop the similarity- and affine-based MLS kernel functions for the case  $\alpha = 1$ , and prove some of their properties.

We will need the following definitions:

$$\begin{aligned} R(w, z) &= |w - z|^{-2} \\ A_0(z) &= \oint_S R(w, z) ds \\ A_1(z) &= \oint_S w R(w, z) ds \\ A_2(z) &= \oint_S w^2 R(w, z) ds \\ B_2(z) &= \oint_S |w|^2 R(w, z) ds \end{aligned}$$

**Theorem A.1.** *The complex similarity-based MLS kernel (up to normalization) is*

$$K_{SMLS}(w, z) = \frac{Q(z)}{w - z} - \frac{P}{|w - z|^2}$$

where

$$Q(z) = \oint_S \frac{1}{w - z} ds$$

and  $P$  is the length of the contour  $S$ .

**Proof.** For a given interior point  $z$ , we first solve a weighted least-squares problem for an optimal similarity transformation  $S_z(w) = aw + b$ . Representing  $S_z$  as the coefficient vector  $s_z = [a \ b]^t$ :

$$s_z = \operatorname{argmin} \oint_S R(w, z) |[w \ 1]s_z - f(w)|^2 ds$$

The solution is given by the normal equation:

$$0 = \oint_S R(w, z) ([w \ 1]^* [w \ 1] s_z - [w \ 1]^* f(w)) ds$$

Since  $s_z$  is a constant within the integral, the solution is simply

$$s_z = T^{-1}(z) \oint_S R(w, z) [w \ 1]^* f(w) ds$$

where  $T(z)$  is the  $2 \times 2$  matrix

$$T(z) = \oint_S R(w, z) [w \ 1]^* [w \ 1] ds = \begin{pmatrix} B_2(z) & \overline{A_1(z)} \\ A_1(z) & A_0(z) \end{pmatrix}$$

Once  $s_z$  is known, we apply it to  $z$  to obtain  $f(z)$ :

$$f(z) = [z \ 1]s_z = [z \ 1]T^{-1}(z) \oint_S R(w, z) [w \ 1]^* f(w) ds \quad (\text{A.1})$$

Now, since  $f(z)$  should also be obtained through the kernel function:

$$f(z) = \oint_S K_{SMLS}(w, z) f(w) ds \tag{A.2}$$

comparing (A.1) and (A.2) yields:

$$K_{SMLS}(w, z) = \begin{pmatrix} z & 1 \end{pmatrix} \begin{pmatrix} B_2(z) & \overline{A_1(z)} \\ A_1(z) & A_0(z) \end{pmatrix}^{-1} \begin{pmatrix} \overline{w} \\ 1 \end{pmatrix} R(w, z)$$

Thus (dropping the variables  $w$  and  $z$  for clarity)

$$\begin{aligned} K_{SMLS}(w, z) &= \begin{pmatrix} z & 1 \end{pmatrix} \begin{pmatrix} B_2 & \overline{A_1} \\ A_1 & A_0 \end{pmatrix}^{-1} \begin{pmatrix} \overline{w}R \\ R \end{pmatrix} = \frac{1}{A_0B_2 - |A_1|^2} \begin{pmatrix} z & 1 \end{pmatrix} \begin{pmatrix} A_0 & -\overline{A_1} \\ -A_1 & B_2 \end{pmatrix} \begin{pmatrix} \overline{w}R \\ R \end{pmatrix} \\ &= \frac{(A_0z - A_1)\overline{w}R + (B_2 - z\overline{A_1})R}{A_0B_2 - |A_1|^2} = \frac{R}{A_0B_2 - |A_1|^2} (\overline{w}(A_0z - A_1) + (B_2 - z\overline{A_1})) \\ &= \frac{R}{A_0B_2 - |A_1|^2} \left( \overline{w} \oint_S \frac{1}{w-z} ds - \oint_S \frac{\overline{w}}{w-z} ds \right) \\ &= \frac{R}{A_0B_2 - |A_1|^2} \left( (\overline{w-z}) \oint_S \frac{1}{w-z} ds - \oint_S \frac{\overline{w-z}}{w-z} ds \right) \end{aligned}$$

Ignoring the normalization constant  $A_0B_2 - |A_1|^2$ ,

$$\begin{aligned} &= \left( \frac{1}{w-z} \oint_S \frac{1}{w-z} ds - \frac{1}{|w-z|^2} \oint_S 1 ds \right) \\ &= \frac{Q(z)}{w-z} - \frac{P}{|w-z|^2} \quad \square \end{aligned}$$

**Theorem A.2.** The real affine-based MLS kernel (up to normalization) is, after a suitable similarity transformation of the plane:

$$K_{AMLS}(w, z) = \frac{1}{|w-z|^2} + \frac{2 \operatorname{Re}(\hat{B}_2(z)w\bar{z} - \hat{A}_2(z)wz)}{\hat{B}_2^2(z) - \hat{A}_2^2(z)} \frac{1}{|w-z|^2}$$

where

$$\hat{A}_2(z) = \oint_S \frac{\overline{w}}{w-z} ds, \quad \hat{B}_2(z) = \oint_S \frac{w}{w-z} ds$$

after the transformation.

**Proof.** Similarly to the proof of Theorem A.1, for a given interior point  $z$ , we first solve a weighted least-squares problem for an optimal affine transformation  $A_z(w) = aw + b\bar{w} + c$ . Representing  $A_z$  as the coefficient vector  $a_z = [a \ b \ c]^t$ :

$$a_z = \operatorname{argmin} \oint_S R(w, z) |[w \ \overline{w} \ 1]a_z - f(w)|^2 ds$$

leads to the kernel

$$K_{AMLS}(w, z) = \begin{pmatrix} z & \overline{z} & 1 \end{pmatrix} T^{-1}(z) \begin{pmatrix} \overline{w} \\ w \\ 1 \end{pmatrix} R(w, z)$$

where  $T$  is the  $3 \times 3$  matrix:

$$T(z) = \begin{pmatrix} B_2(z) & \overline{A_2(z)} & \overline{A_1(z)} \\ A_2(z) & B_2(z) & A_1(z) \\ A_1(z) & \overline{A_1(z)} & A_0(z) \end{pmatrix}$$

Using the minors

$$\begin{aligned} T_{11} &= A_0 B_2 - |A_1|^2 \\ T_{21} &= A_0 \overline{A_2} - \overline{A_1}^2 \\ T_{31} &= A_1 \overline{A_2} - B_2 \overline{A_1} \\ T_{33} &= B_2^2 - |A_2|^2 \end{aligned}$$

we obtain

$$M_A(w, z) = \frac{(T_{33} + 2 \operatorname{Re}(T_{31}(w + z) + T_{11}w\bar{z} - T_{21}wz))R(w, z)}{|T|}$$

Consider the simplifying similarity transformation  $f(z) = pz + q$ , where  $p$  and  $q$  are the complex numbers (depending on  $z$ ):

$$p(z) = A_0 \exp\left(-\frac{i}{2} \arg(A_0 A_2 - A_1^2)\right), \quad q(z) = -\frac{A_1}{A_0}.$$

This will transform the functions into new ones, which we will denote using a hat, e.g.  $\hat{A}_0$ . It is easy to see that after this transformation we have  $\hat{A}_0 = 1$ ,  $\hat{A}_1 = 0$ , and  $\operatorname{Im}(\hat{A}_2) = 0$ , thus

$$\begin{aligned} \hat{T}_{11} &= \hat{B}_2 \\ \hat{T}_{21} &= \hat{A}_2 \\ \hat{T}_{31} &= 0 \\ \hat{T}_{33} &= \hat{B}_2^2 - \hat{A}_2^2 \\ |\hat{T}| &= \hat{T}_{33} \end{aligned}$$

$$K_{AMLS}(w, z) = R(w, z) + \frac{2R(w, z) \operatorname{Re}(\hat{B}_2(z)w\bar{z} - \hat{A}_2(z)wz)}{\hat{B}_2^2(z) - \hat{A}_2^2(z)}$$

Now observe that

$$\begin{aligned} \hat{B}_2(z) &= \oint_S |w|^2 R(w, z) ds = \oint_S \frac{w\bar{w}}{(w-z)(\bar{w}-\bar{z})} ds = \oint_S \frac{(w-z+z)\bar{w}}{(w-z)(\bar{w}-\bar{z})} ds \\ &= \oint_S \frac{\bar{w}}{w-z} ds + z \oint_S \frac{\bar{w}}{|w-z|^2} ds = \oint_S \frac{\bar{w}}{w-z} ds + z\bar{A}_1 = \oint_S \frac{w}{w-z} ds \end{aligned}$$

and similarly

$$\hat{A}_2(z) = \oint_S \frac{\bar{w}}{w-z} ds \quad \square$$

We now show that both the similarity-based and affine-based MLS kernels with  $\alpha = 1$  are pseudo-harmonic. First a technical lemma:

**Lemma A.1.** On the unit circle  $C$ , for any integer  $k \geq 0$ ,

$$\oint_C \frac{w^k}{|w-z|^2} ds = \frac{2\pi z^k}{1-|z|^2} \quad \text{and} \quad \oint_C \frac{\bar{w}^k}{|w-z|^2} ds = \frac{2\pi \bar{z}^k}{1-|z|^2}$$

**Proof.** For the unit circle we have  $\bar{w} = 1/w$ ,  $|w| = 1$  and  $ds = \frac{dw}{iw}$ . Thus

$$\oint_C \frac{w^k}{|w-z|^2} ds = -i \oint_C \frac{w^k}{w(w-z)(\bar{w}-\bar{z})} dw = -i \oint_C \frac{w^k}{(w-z)(1-\bar{z}w)} dw$$

Now  $f_z(w) = \frac{w^k}{(w-z)(1-\bar{z}w)}$  is an analytic function of  $w$  with a pole at  $w = z$  inside  $C$ , and a pole at  $w = 1/\bar{z}$ , outside  $C$ . Thus, by the Cauchy residue theorem,

$$= 2\pi i \operatorname{Res}(f_z, 0) = 2\pi \frac{z^k}{1 - |z|^2}.$$

The second identity follows by conjugation of the first identity.

The observant reader will notice that this Lemma is actually also a consequence of the fact that the Poisson kernel reproduces harmonic functions on the unit circle. Thus it also reproduces holomorphic functions (since both the real and imaginary parts of a holomorphic function are harmonic), including  $w^k$ . □

**Theorem A.3.** Both the similarity- and affine-based MLS kernel functions are pseudo-harmonic.

**Proof.** Applying Lemma A.1 to the case where  $S = C$  is the unit circle, we have:

$$\begin{aligned} c(z) &= \frac{2\pi}{1 - |z|^2} \\ A_0(z) &= \oint_C R(w, z) ds = c(z) \\ A_1(z) &= \oint_C w R(w, z) ds = c(z)z \\ A_2(z) &= \oint_C w^2 R(w, z) ds = c(z)z^2 \\ B_2(z) &= \oint_C |w|^2 R(w, z) ds = A_0 = c(z) \end{aligned}$$

Thus, for the similarity case:

$$\begin{aligned} Q(z) &= \oint_C \frac{1}{w - z} ds = \oint_C (w - z) R(w, z) ds = \oint_C w R(w, z) ds - z \oint_C R(w, z) ds \\ &= A_1(z) - z A_0(z) = 0 \end{aligned}$$

And for the affine case, similar calculations show that the similarity transformation of the plane used in Theorem A.2 has parameters  $p(z) = 0, q(z) = -z$ , thus is just a translation, not changing the influence function  $R$ . And, since  $z$  is translated to 0, we have

$$\hat{B}_2(z)w\bar{z} - \hat{A}_2(z)wz = 0$$

namely, both the similarity and affine cases result in the Poisson kernel. □

To complete the picture for the MLS kernels, we provide closed expressions for the required integrals in the case that the contour  $S$  is a polygon.

**Theorem A.4.** If  $S$  is an  $n$ -sided polygon with vertices  $(w_1, \dots, w_n)$ , denote (for cyclic indices  $w_{n+1} \equiv w_1$ ):

$$\begin{aligned} u_j &= \frac{w_{j+1} - w_j}{|w_{j+1} - w_j|}, & a_j &= \overline{u_j}^2, & b_j &= \frac{w_{j+1}\overline{w_j} - w_j\overline{w_{j+1}}}{w_{j+1} - w_j} = \frac{2i \operatorname{Im}(w_j\overline{w_{j+1}})}{w_j - w_{j+1}} \\ r_j(z) &= \frac{w_{j+1} - z}{w_j - z}, & \beta_j(z) &= \frac{\sqrt{a_j}}{a_j z + b_j - \bar{z}} = \frac{-i|w_{j+1} - w_j|}{2 \operatorname{Im}(w_{j+1} - w_j z - w_j\overline{w_{j+1}})} \end{aligned}$$

Then:

$$\begin{aligned} A_0(z) &= \sum_{j=1}^n \beta_j(z) (\log r_j(z) - \log \overline{r_j(z)}) \\ A_1(z) &= \sum_{j=1}^n \beta_j(z) (z \log r_j(z) - \overline{(a_j z + b_j)} \log \overline{r_j(z)}) \\ A_2(z) &= \sum_{j=1}^n \overline{a_j} |w_{j+1} - w_j| + \beta_j(z) (z^2 \log r_j(z) - \overline{(a_j z + b_j)}^2 \log \overline{r_j(z)}) \end{aligned}$$

$$Q(z) = \sum_{j=1}^n u_j \log \overline{r_j(z)}$$

$$\hat{B}_2(z) = \hat{P} + z \sum_{j=1}^n \overline{u_j} \log r_j(z) = \hat{P} + z \hat{Q}(z)$$

$$\hat{A}_2(z) = \sum_{i=1}^n \overline{a_j} |w_{j+1} - w_j| + \overline{u_j} (a_j z + b_j) \log r_j(z)$$

where  $\hat{P}$  is the total length of the transformed polygon edges and  $\hat{Q}$  is the transformed version of  $Q$ .

**Proof.** Note that for a line segment  $[w_j, w_{j+1}]$ , we may write for any  $w$  on the segment:  $\overline{w} = a_j w + b_j$  for the complex constants  $a_j, b_j$  defined above. Thus  $d\overline{w} = \overline{u_j}^2 dw$  and  $ds = \overline{u_j} dw$ . The results follow by straightforward integration.  $\square$

**Appendix B**

**Table B.1**

Error measure  $E_1$  ( $\times 100$ ) – the relative  $l_2$  difference between the barycentric coordinate function and the harmonic (H) coordinate function (\* denotes  $> 10^4$ ). Red rows correspond to the coordinate functions in Figs. 2–6. Minimal values for each coordinate function are in bold. (For interpretation of the references to color in this table, the reader is referred to the web version of this article.)

	W	MV	L	H	MLS	P	ME	GW	PGW
Square									
Average	<b>0</b>	<b>0.04</b>	<b>0</b>	<b>0</b>	<b>0.00</b>	<b>0.02</b>	<b>0</b>	<b>0.08</b>	<b>0.08</b>
Circle									
Average	<b>12.3</b>	2.03	<b>12.4</b>	<b>0</b>	<b>0</b>	<b>0</b>	<b>1.71</b>	<b>0</b>	<b>12.0</b>
Convex Pentagon									
1	<b>19.0</b>	<b>0.23</b>	<b>7.52</b>	<b>0</b>	<b>0.19</b>	<b>0.17</b>	<b>2.14</b>	<b>1.29</b>	<b>0.35</b>
2	26.1	0.28	10.3	0	0.24	<b>0.17</b>	2.65	1.53	0.42
3	1.26	0.18	0.38	0	<b>0.04</b>	0.16	1.50	0.88	0.42
4	0.71	0.11	0.21	0	<b>0.03</b>	0.11	0.95	0.56	0.26
5	0.11	0.00	0.04	0	<b>0.00</b>	0.00	0.03	0.02	0.01
Average	9.44	0.16	3.69	0	<b>0.10</b>	0.12	1.45	0.86	0.29
Non-convex Man 1									
1	*	0.31	*	0	0.46	0.73	2.06	6.43	
2	*	0.86	*	0	<b>0.30</b>	1.09	1.37	2.08	3.74
3	*	1.42	*	0	<b>0.81</b>	2.64	1.09	2.10	7.70
4	*	<b>2.12</b>	*	0	3.69	2.76	5.00	7.69	11.1
5	*	3.85	*	0	3.90	3.44	<b>2.79</b>	10.5	4.81
6	621	1.98	*	0	<b>0.67</b>	1.89	1.18	3.08	0.96
7	983	1.52	*	0	<b>0.86</b>	1.48	1.20	1.87	0.96
8	*	<b>3.02</b>	*	0	<b>3.25</b>	<b>2.88</b>	<b>3.04</b>	<b>10.7</b>	<b>3.66</b>
9	*	1.05	*	0	1.83	<b>0.99</b>	3.07	4.85	6.40
10	*	<b>0.52</b>	*	0	1.09	0.72	2.30	1.85	0.79
11	*	0.81	*	0	0.72	<b>0.58</b>	1.89	6.37	6.63
12	*	1.36	*	0	2.17	1.42	<b>1.10</b>	3.12	1.54
13	*	3.89	*	0	5.74	<b>3.76</b>	3.83	13.9	6.70
14	*	3.85	*	0	4.33	3.78	<b>3.26</b>	13.2	6.14
15	*	<b>0.95</b>	*	0	2.46	1.07	1.21	1.36	2.24
16	410	0.51	*	0	0.54	<b>0.32</b>	1.44	3.81	4.84
17	*	0.36	*	0	0.46	0.40	2.00	1.38	<b>0.27</b>
18	*	<b>1.75</b>	*	0	2.38	1.77	2.74	2.67	5.83
19	*	7.46	*	0	4.06	7.36	<b>3.75</b>	16.3	6.27
20	*	3.25	*	0	<b>1.51</b>	3.10	2.65	3.21	2.34
21	*	3.13	*	0	<b>0.71</b>	2.95	1.85	4.26	1.50
22	*	5.73	*	0	4.61	5.09	<b>3.11</b>	11.3	4.03
23	*	<b>2.84</b>	*	0	4.46	4.02	5.99	8.89	14.3
24	*	1.12	*	0	<b>0.62</b>	1.78	0.66	1.77	7.00
25	*	0.62	*	0	<b>0.30</b>	0.78	1.17	1.42	4.24
Average	*	2.17	*	0	<b>2.06</b>	2.26	2.34	5.59	4.82
Non-convex Man 2									
1	194	0.31	*	0	<b>0.06</b>	0.46	0.80	1.99	7.70
2	*	0.85	*	0	<b>0.32</b>	1.09	1.49	2.05	5.84
3	*	1.41	*	0	<b>0.85</b>	2.64	1.15	2.08	8.92
4	*	<b>2.13</b>	*	0	3.71	2.77	5.20	7.68	13.4

(continued on next page)

Table B.1 (continued)

	W	MV	L	H	MLS	P	ME	GW	PGW
5	*	3.69	*	0	3.88	3.30	2.70	9.50	<b>1.85</b>
6	240	1.91	*	0	<b>0.77</b>	1.82	1.30	2.80	1.24
7	*	1.45	*	0	<b>0.97</b>	1.41	1.35	1.76	1.07
8	*	3.26	*	0	3.52	3.12	<b>3.00</b>	11.0	3.49
9	*	1.04	*	0	1.49	<b>0.98</b>	3.13	4.49	5.63
10	*	<b>0.42</b>	*	0	1.02	0.61	2.40	1.46	0.71
11	417	0.71	*	0	0.64	<b>0.52</b>	1.78	5.89	6.09
12	*	<b>0.93</b>	*	0	2.06	0.99	0.96	2.37	1.26
13	*	3.33	*	0	5.10	<b>3.24</b>	3.98	12.5	6.44
14	*	1.55	*	0	5.19	<b>1.49</b>	3.26	8.28	2.41
15	*	<b>0.62</b>	*	0	2.42	0.66	1.98	1.22	3.31
16	*	0.37	*	0	0.44	<b>0.21</b>	1.48	3.16	4.55
17	*	0.30	*	0	0.24	0.29	1.20	1.20	<b>0.18</b>
18	*	<b>3.09</b>	*	0	<b>5.41</b>	<b>3.18</b>	<b>3.87</b>	<b>4.83</b>	<b>8.30</b>
19	*	6.58	*	0	7.13	6.50	<b>3.84</b>	15.5	12.6
20	*	8.10	*	0	<b>2.28</b>	8.35	<b>6.84</b>	11.5	9.59
21	*	17.4	*	0	7.89	17.5	<b>3.97</b>	18.3	15.7
22	*	9.89	*	0	5.87	9.62	<b>2.45</b>	11.1	6.70
23	729	5.99	*	0	<b>0.74</b>	6.02	2.79	9.97	3.45
24	*	5.89	*	0	4.98	5.24	2.78	11.3	6.62
25	*	<b>2.78</b>	*	0	4.53	3.96	6.14	8.92	16.4
26	329	1.16	*	0	<b>0.65</b>	1.76	0.68	1.76	8.29
27	222	0.62	*	0	<b>0.30</b>	0.78	1.16	1.42	4.20
Average	*	3.17	*	0	2.68	3.28	<b>2.66</b>	6.44	6.15

Table B.2

Error measure  $E_2 (\times 100)$  – the relative absolute difference between the Dirichlet energy of the barycentric coordinate function and the Dirichlet energy of the harmonic (H) coordinate function (\* denotes  $> 10^4$ ). Red rows correspond to the coordinate functions in Figs. 2–6. Minimal values for each coordinate function are in bold. (For interpretation of the references to color in this table, the reader is referred to the web version of this article.)

	W	MV	L	H	MLS	P	ME	GW	PGW
Square									
Average	<b>0</b>	<b>0.65</b>	<b>0</b>	<b>0</b>	<b>0.02</b>	<b>0.27</b>	<b>0</b>	<b>1.30</b>	<b>1.30</b>
Circle									
Average	<b>98.2</b>	<b>8.77</b>	<b>98.4</b>	<b>0</b>	<b>0</b>	<b>0</b>	<b>10.1</b>	<b>0</b>	<b>39.8</b>
Convex Pentagon									
1	<b>67.1</b>	<b>1.41</b>	<b>33.9</b>	<b>0</b>	<b>0.63</b>	<b>0.66</b>	<b>20.0</b>	<b>5.90</b>	<b>3.56</b>
2	78.4	1.66	39.9	0	0.71	<b>0.66</b>	23.0	6.52	4.18
3	4.82	1.37	1.80	0	<b>0.29</b>	0.67	13.5	3.80	2.97
4	3.64	1.06	1.30	0	<b>0.23</b>	0.54	10.5	3.01	2.31
5	3.15	0.11	1.52	0	<b>0.04</b>	0.07	1.44	0.46	0.26
Average	31.4	1.12	15.7	0	<b>0.38</b>	0.52	13.7	3.94	2.66
Non-convex Man 1									
1	*	2.97	*	0	<b>0.63</b>	2.68	5.10	30.4	20.4
2	*	3.82	*	0	<b>1.10</b>	3.51	9.44	12.9	23.6
3	*	6.23	*	0	<b>4.79</b>	8.50	8.21	9.14	33.9
4	*	<b>4.74</b>	*	0	5.84	5.28	20.6	34.0	21.3
5	*	4.83	*	0	8.66	<b>4.49</b>	22.3	34.1	18.7
6	*	3.01	*	0	<b>1.28</b>	2.80	14.6	7.91	3.88
7	*	2.86	*	0	<b>1.67</b>	2.79	14.4	5.80	4.25
8	*	<b>7.21</b>	*	0	<b>7.83</b>	<b>6.92</b>	<b>26.2</b>	<b>47.8</b>	<b>16.4</b>
9	*	3.74	*	0	4.99	<b>3.58</b>	16.3	26.2	22.6
10	*	<b>2.20</b>	*	0	2.94	2.51	19.3	11.4	3.91
11	*	2.22	*	0	2.06	<b>1.44</b>	17.1	23.9	20.6
12	*	6.25	*	0	7.26	<b>6.25</b>	7.38	19.1	7.91
13	*	7.04	*	0	9.56	<b>6.71</b>	15.0	44.4	21.5
14	*	6.76	*	0	8.45	<b>6.52</b>	16.6	39.9	18.0
15	*	<b>5.39</b>	*	0	7.74	5.51	6.53	13.6	10.3
16	*	1.86	*	0	1.89	<b>1.10</b>	14.7	13.9	13.9
17	*	1.61	*	0	1.92	<b>1.47</b>	17.0	9.29	2.30
18	*	6.60	*	0	7.90	<b>6.59</b>	13.4	16.0	18.8
19	*	14.9	*	0	<b>9.02</b>	14.7	28.8	58.7	40.9
20	*	3.99	*	0	<b>2.81</b>	3.90	19.4	5.66	8.36
21	*	3.81	*	0	<b>1.08</b>	3.58	18.2	8.51	5.86
22	*	7.10	*	0	10.6	<b>6.59</b>	23.0	37.2	18.4
23	*	<b>5.74</b>	*	0	6.34	6.61	21.0	35.9	28.0

(continued on next page)

Table B.2 (continued)

	W	MV	L	H	MLS	P	ME	GW	PGW
24	*	6.41	*	0	<b>5.66</b>	7.92	6.03	10.7	36.8
25	*	3.49	*	0	<b>1.34</b>	3.20	7.60	11.3	25.3
Average	*	4.99	*	0	<b>4.93</b>	5.01	15.5	22.7	17.8
Non-convex Man 2									
1	*	2.97	*	0	<b>0.70</b>	2.68	5.33	29.8	23.6
2	*	3.81	*	0	<b>1.17</b>	3.50	9.99	12.7	31.6
3	*	6.22	*	0	<b>5.03</b>	8.50	8.55	9.11	36.1
4	*	<b>4.76</b>	*	0	5.77	5.33	21.2	33.4	25.7
5	*	4.71	*	0	8.78	<b>4.38</b>	21.5	35.1	8.86
6	*	2.95	*	0	<b>1.43</b>	2.74	14.9	7.52	5.10
7	*	2.81	*	0	<b>1.83</b>	2.74	14.4	5.71	4.58
8	*	7.61	*	0	8.57	<b>7.32</b>	24.5	48.9	22.6
9	*	3.49	*	0	4.29	<b>3.34</b>	17.5	23.7	19.7
10	*	<b>1.95</b>	*	0	3.08	2.26	19.8	10.2	3.95
11	*	2.09	*	0	2.05	<b>1.42</b>	16.1	25.2	19.3
12	*	5.31	*	0	7.54	<b>5.30</b>	7.05	19.7	7.01
13	*	7.07	*	0	9.45	<b>6.67</b>	21.0	46.6	24.4
14	*	3.83	*	0	12.4	<b>3.67</b>	18.0	34.2	9.99
15	*	<b>3.04</b>	*	0	6.73	3.05	10.4	8.11	11.1
16	*	1.70	*	0	2.06	<b>0.99</b>	16.1	16.5	16.3
17	*	1.52	*	0	1.65	<b>1.35</b>	14.7	10.4	2.14
18	*	<b>25.8</b>	*	0	<b>28.3</b>	<b>27.0</b>	<b>15.3</b>	<b>54.3</b>	<b>32.0</b>
19	*	14.2	*	0	15.9	<b>14.0</b>	26.9	57.7	49.2
20	*	13.8	*	0	<b>3.38</b>	14.8	30.1	30.7	34.0
21	*	<b>11.5</b>	*	0	12.0	11.7	13.7	15.3	45.8
22	*	9.26	*	0	<b>8.98</b>	9.43	12.7	13.9	13.1
23	*	16.6	*	0	<b>1.27</b>	17.4	26.0	39.7	23.9
24	*	7.12	*	0	11.6	<b>6.69</b>	21.2	34.0	25.7
25	*	<b>5.89</b>	*	0	6.53	6.76	22.2	38.2	31.8
26	*	6.49	*	0	6.20	8.02	<b>6.06</b>	10.8	44.2
27	*	3.49	*	0	<b>1.45</b>	3.19	7.40	12.0	26.8
Average	*	6.67	*	0	<b>6.60</b>	6.83	16.4	25.3	22.2

Table B.3

Error measure  $E_3 (\times 10^6)$  – the  $l_2$  norm of the Laplacian of the barycentric coordinate function (\* denotes  $> 1000$ ). Red rows correspond to the coordinate functions in Figs. 2–6. Minimal values for each coordinate function are in bold. (For interpretation of the references to color in this table, the reader is referred to the web version of this article.)

	W	MV	L	H	MLS	P	ME	GW	PGW
Square									
Average	<b>0</b>	<b>0.08</b>	<b>0</b>	<b>0</b>	<b>0.02</b>	<b>0.03</b>	<b>0</b>	<b>0.13</b>	<b>0.14</b>
Circle									
Average	255	16.7	256	0	0	0	22.1	0	60.6
Convex Pentagon									
1	120	4.38	97.8	0	<b>1.48</b>	1.94	58.2	10.4	13.2
2	103	3.90	84.5	0	<b>1.26</b>	1.63	50.1	8.90	11.7
3	4.52	2.38	2.18	0	<b>0.51</b>	0.78	19.4	4.23	5.43
4	3.59	1.91	1.59	0	<b>0.42</b>	0.64	15.7	3.44	4.36
5	1.46	0.07	1.12	0	<b>0.02</b>	0.03	0.90	0.18	0.20
Average	46.6	2.53	37.4	0	<b>0.74</b>	1.01	28.9	5.43	6.98
Non-convex Man 1									
1	*	3.73	*	0	<b>0.94</b>	2.58	6.74	58.3	19.2
2	*	3.43	*	0	<b>1.13</b>	2.66	10.1	23.7	24.4
3	360	5.20	*	0	<b>4.62</b>	5.81	9.01	10.1	29.0
4	*	16.2	*	0	<b>13.4</b>	16.3	139	193	104
5	*	16.9	*	0	29.7	<b>16.3</b>	193	224	168
6	114	4.73	*	0	<b>3.16</b>	4.27	60.5	19.8	12.6
7	170	4.59	*	0	<b>3.11</b>	4.32	51.8	14.8	12.0
8	*	<b>25.4</b>	*	0	<b>23.9</b>	<b>24.6</b>	<b>199</b>	<b>304</b>	<b>183</b>
9	*	9.40	*	0	<b>8.13</b>	9.14	56.6	86.6	59.2
10	484	2.69	*	0	2.49	<b>2.44</b>	29.7	15.8	6.16
11	217	2.42	*	0	2.48	<b>1.59</b>	31.1	34.2	20.3
12	*	9.77	*	0	<b>8.75</b>	9.48	15.9	38.5	18.1
13	*	15.9	*	0	<b>15.0</b>	15.1	51.2	121	104
14	*	17.0	*	0	20.3	<b>16.2</b>	85.9	201	91.9
15	*	9.81	*	0	9.34	<b>9.37</b>	13.1	38.4	16.8

(continued on next page)

Table B.3 (continued)

	W	MV	L	H	MLS	P	ME	GW	PGW
16	66.1	2.44	*	0	2.29	<b>1.51</b>	24.3	21.4	13.1
17	412	1.96	*	0	2.17	<b>1.46</b>	24.5	16.1	4.83
18	*	17.5	*	0	<b>17.0</b>	17.3	56.2	58.8	49.7
19	*	45.3	*	0	<b>26.5</b>	44.8	223	301	553
20	*	9.21	*	0	<b>8.19</b>	8.94	106	19.4	30.9
21	*	6.88	*	0	<b>2.99</b>	6.37	95.0	24.9	22.6
22	*	24.5	*	0	40.4	<b>23.4</b>	223	249	188
23	*	15.7	*	0	<b>11.4</b>	16.1	126	156	120
24	805	<b>3.96</b>	*	0	4.29	4.10	5.70	8.37	23.3
25	*	2.89	*	0	<b>1.16</b>	2.09	7.30	17.4	21.4
Average	*	11.1	*	0	<b>10.5</b>	10.7	73.7	90.2	75.8
Non-convex Man 2									
1	85.1	3.64	*	0	<b>1.03</b>	2.65	6.23	52.8	19.8
2	808	3.35	*	0	<b>1.21</b>	2.67	9.76	19.0	27.4
3	*	4.98	*	0	<b>4.80</b>	5.62	8.81	9.64	25.9
4	*	14.6	*	0	<b>11.4</b>	14.9	125	135	104
5	*	17.8	*	0	33.7	<b>17.3</b>	203	257	107
6	75.2	5.00	375	0	<b>3.39</b>	4.52	66.9	20.9	17.8
7	*	4.94	*	0	<b>3.48</b>	4.67	55.1	14.8	11.9
8	*	25.6	*	0	27.4	<b>24.7</b>	220	314	367
9	*	10.4	*	0	<b>9.39</b>	10.0	78.9	85.4	63.5
10	483	2.29	*	0	2.68	<b>2.22</b>	28.5	16.6	6.10
11	72.0	2.52	432	0	2.63	<b>1.79</b>	30.5	36.6	17.7
12	511	8.87	*	0	9.36	<b>8.56</b>	17.8	46.6	16.4
13	*	19.7	*	0	20.6	<b>18.1</b>	102	179	131
14	*	16.1	*	0	43.3	<b>15.0</b>	143	152	75.2
15	*	8.42	*	0	10.4	<b>8.13</b>	32.7	27.7	22.6
16	186	2.33	*	0	2.79	<b>1.51</b>	32.0	22.4	15.5
17	609	2.34	*	0	2.72	<b>1.89</b>	36.4	19.6	5.31
18	*	<b>83.8</b>	*	0	<b>116</b>	<b>87.2</b>	<b>85.2</b>	<b>214</b>	<b>153</b>
19	*	51.0	*	0	53.2	<b>50.3</b>	224	329	470
20	*	155	904	0	<b>31.0</b>	170	638	360	448
21	*	<b>40.0</b>	*	0	40.3	40.8	121	63.5	205
22	*	38.5	*	0	33.4	<b>39.7</b>	201	65.9	107
23	240	105	896	0	<b>6.16</b>	112	346	266	208
24	*	28.7	*	0	43.4	<b>28.0</b>	212	218	215
25	*	15.1	*	0	<b>11.2</b>	15.7	113	130	133
26	92.6	<b>4.37</b>	*	0	5.04	4.60	5.18	8.93	29.7
27	77.4	2.80	621	0	<b>1.44</b>	2.13	6.63	15.8	24.0
Average	*	25.1	*	0	<b>19.7</b>	25.7	117	114	112

## References

- Ahlfors, L., 1979. *Complex Analysis*, 3rd ed. McGraw-Hill.
- Belyaev, A., 2006. On transfinite barycentric coordinates. In: *Proc. Symp. Geometry Processing*, pp. 89–99.
- Belyaev, A., Fayolle, P., 2015. On transfinite Gordon–Wixom interpolation schemes and their extensions. *Comput. Graph.* 51 (C), 74–80. <http://dx.doi.org/10.1016/j.cag.2015.05.010>.
- Ben-Chen, M., Weber, O., Gotsman, C., 2009. Variational harmonic maps for space deformation. In: *Proc. SIGGRAPH. ACM Trans. Graph.* 28 (3).
- Dyken, C., Floater, M., 2009. Transfinite mean value interpolation. *Comput. Aided Geom. Des.* 26 (1), 117–134.
- Floater, M., 2003. Mean-value coordinates. *Comput. Aided Geom. Des.* 20 (1), 19–27.
- Floater, M., 2015. Generalized barycentric coordinates and applications. *Acta Numer.* 24, 161–214.
- Floater, M., Hormann, K., Kós, G., 2006. A general construction of barycentric coordinates over convex polygons. *Adv. Comput. Math.* 24, 311–331.
- Gordon, W.J., Wixom, J.A., 1974. Pseudo-harmonic interpolation on convex domains. *SIAM J. Numer. Anal.* 11, 909–933.
- Hormann, K., Floater, M.S., 2006. Mean value coordinates for arbitrary planar polygons. *ACM Trans. Graph.* 25, 1424–1441.
- Hormann, K., Sukumar, N., 2008. Maximum entropy coordinates for arbitrary polytopes. *Comput. Graph. Forum* 27, 1513–1520.
- Joshi, P., Meyer, M., DeRose, T., Green, B., Sanocki, T., 2007. Harmonic coordinates for character articulation. *ACM Trans. Graph.* 26 (3). <http://dx.doi.org/10.1145/1276377.1276466>.
- Kosinka, J., Barton, M., 2016. Convergence of barycentric coordinates to barycentric kernels. *Comput. Aided Geom. Des.* 43, 200–210.
- Li, X.-Y., Hu, S.-M., 2013. Poisson coordinates. *IEEE Trans. Vis. Comput. Graph.* 19 (2), 344–352.
- Lipman, Y., Levin, D., Cohen-Or, D., 2008. Green coordinates. *ACM Trans. Graph.* 27 (3). <http://dx.doi.org/10.1145/1360612.1360677>.
- Manson, J., Schaefer, S., 2010. Moving least squares coordinates. *Comput. Graph. Forum* 29 (5), 1517–1524.
- Manson, J., Li, K., Schaefer, S., 2011. Positive Gordon–Wixom coordinates. *Comput. Aided Des.* 43 (11), 1422–1426.
- Martin, S., Kaufmann, P., Botsch, M., Wicke, M., Gross, M., 2008. Polyhedral finite elements using harmonic basis functions. In: *Proc. Symp. Geom. Process. Comput. Graph. Forum* 27 (5), 1521–1529.
- Pinkall, U., Polthier, K., 1993. Computing discrete minimal surfaces and their conjugates. *Exp. Math.* 2 (1), 15–36.
- Schaefer, S., Ju, T., Warren, J., 2007. A unified, integral construction for coordinates over closed curves. *Comput. Aided Geom. Des.* 24 (8–9), 481–493.
- Schneider, T., Hormann, K., 2015. Smooth bijective maps between arbitrary planar polygons. *Comput. Aided Geom. Des.* 35–36, 243–254.

- Sukumar, N., 2004. Construction of polygonal interpolants: a maximum entropy approach. *Int. J. Numer. Methods Eng.* 61 (12), 2159–2181.
- Wachspress, E.L., 1975. A Rational Finite Element Basis. *Mathematics in Science and Engineering*, vol. 114. Academic Press.
- Weber, O., Ben-Chen, M., Gotsman, C., 2009. Complex barycentric coordinates with applications to image deformation. In: *Proc. Eurographics. Comput. Graph. Forum* 28 (2), 587–597.
- Weber, O., Ben-Chen, M., Gotsman, C., Hormann, K., 2011. A complex view of barycentric mappings. In: *Proc. Symp. Geometry Process. Comput. Graph. Forum* 30 (5), 1533–1542.
- Weber, O., Gotsman, C., 2010. Controllable conformal mappings for shape deformation and interpolation. In: *Proc. SIGGRAPH. ACM Trans. Graph.* 29 (4).